Ab initio and empirical modeling of lithium atoms penetration into silicon

CrossMark

Natalia S. Mikhaleva [a,b], Maxim A. Visotin [b,*], Zakhar I. Popov [a,c], Alexander A. Kuzubov [a,b], Alexander S. Fedorov [a,b]

[a] L.V. Kirensky Institute of Physics SB RAS, 50 bld. 38 Akademgorodok, 660036 Krasnoyarsk, Russia
[b] Siberian Federal University, 79 Svobodny pr., 660041 Krasnoyarsk, Russia
[c] National University of Science and Technology MISiS, 4 Leninskiy pr., 119049 Moscow, Russia

ARTICLE INFO

ABSTRACT

A process of lithium atoms penetration into silicon (1 0 0) subsurface layers was investigated with the help of DFT method. It was shown that, while the concentration of lithium adatoms on reconstructed (1 0 0) silicon surface is low, the bonding energy of lithium atoms in the subsurface layers is smaller than the bonding energy on the surface, so lithium atoms are unlikely to migrate into the crystal. When the (1 0 0) silicon surface is covered by 2 layers of lithium, migration into the subsurface layer becomes favorable. In addition to this, the reconstruction of the surface changes to the form with symmetric dimers as the concentration increases. Thus, all possible lithium migration paths become energy-wise equal, so the rate of lithium atom transfer into silicon crystal rises.

In addition to the ab initio calculations, an ad-hoc empirical interatomic potential was developed and the kinetics of lithium diffusion into silicon were studied. It was shown that lithium penetration proceeds in a layer-by-layer way with a sharp border between undoped and lithiated silicon. This is accounted for the fact that, once a tetrahedral interstice is occupied by a lithium atom, the migration barriers between the adjacent interstices become lower and the rate of diffusion increases.

© 2015 Elsevier B.V. All rights reserved.

1. Introduction

Nowadays, silicon is considered as a promising novel material for Li-ion batteries anodes as it has the highest theoretical specific capacity (4200 mA h/g), which is 11 times higher than in graphite (372 mA h/g) [1–5]. Unfortunately, silicon lithiation is accompanied by a significant (up to 300%) increase in specific volume [2,6,7], as well as phase transitions between different Li_xSi phases. In this process, the change in volume causes large mechanical stresses and, consequently, a break-up of the crystal [8–11]. In addition to this, silicon has a low diffusion coefficient for lithium ions [12,13]. These limitations impede application of bulk silicon in modern Li-ion batteries.

To overcome this obstacle, nanostructured silicon-based materials were suggested, including thin films [14–16], silicon nanowires [17–19], nanoparticles [20–22], nanotubes [23–26] and porous structures [27–33]. Numerous preliminary experimental investigations show encouraging results for the usage of these materials as anodes in Li-ion batteries. Therefore, the theoretical

investigations aiming at lithium diffusion in silicon structures and search for the way to overcome material limitations become utterly relevant.

At first, lithium atoms are adsorbed on the surface and subsequently penetrate subsurface layers. In [34], the average times Li adatom stays atop (1 0 0) and (1 1 1) surfaces were obtained for temperatures in the interval of 800–1250 K and it was shown that Li goes into silicon through (1 0 0) surface easier than through (1 1 1) surface.

The sorption of lithium is greatly affected by the reconstruction of the surface, where it takes place. It is common knowledge that silicon (1 0 0) surface is covered with silicon dimers, which reduces the number of dangling bonds and minimizes the surface energy, leading to the (2×2) reconstruction at room temperature. Theoretical investigations [35] showed that, when silicon (1 0 0) surface is covered with 1 monolayer of lithium, the (2×2) reconstruction is replaced by the (2×1) reconstruction with a symmetrical silicon dimers arrangement. Also, the potential barriers of a single lithium atom transition from surface to subsurface layers and from subsurface layers into the bulk were calculated at dilute lithium concentration (0.88 eV and 0.5 eV, correspondingly). However, the barriers for the diffusion at higher Li concentrations,

---

* Corresponding author. Tel.: +7 983 500 6770.
 E-mail address: visotin.maxim@gmail.com (M.A. Visotin).

when the surface reconstruction changes, have not been studied yet.

In this work, we have investigated the diffusion of lithium through Si (100) surface at different Li concentrations by means of density functional theory (DFT) methods and classical molecular dynamics (MD). First, the possible positions of Li on the surface were found and compared. Then, main paths of Li atom transition into bulk silicon were examined and the effect of Li concentration level on the potential barriers was studied. Finally, we performed MD simulations of Li diffusion through Si (100) surface and estimated the diffusion coefficient.

2. DFT calculations of lithium atoms behavior on silicon surface and their jumps into the subsurface layers

All the calculations of lithium sorption on the surface and the barriers of transition into the subsurface layers were conducted with VASP 5.3 (Vienna Ab-initio Simulation Package) [36–38] quantum-chemical software package using DFT [39,40] in plane-wave basis sets and with the help of projector augmented wave (PAW) method [41,42]. General gradient approximation (GGA) in Perdew–Burke–Ernzerhof (PBE) form [43] with Grimme van der Waals corrections was used [44]. The nudged elastic band (NEB) method [45] was applied for modeling transitional states and finding potential barriers for Li atom jumps.

Before the actual studies, a cubic unit cell of silicon was modeled. During its structural optimization, a $12 \times 12 \times 12$ Monkhorst–Pack mesh [46] was used for Brillouin zone (BZ) integrations. The resulting unit cell was used to build up a $4 \times 4 \times 3$ supercell in a form of a periodic slab, which was subsequently used for modeling silicon (100) surface with the $c(4 \times 2)$ reconstruction. The supercell dimensions were $a = 15.3724$ Å, $b = c = 21.54$ Å. Considering relatively large supercell sizes, the density of k-points was decreased, resulting in a $2 \times 2 \times 1$ BZ mesh. In order to prevent slabs from interacting with each other (supercell's periodic images), they were separated by 27 Å vacuum spacings.

The thickness of the slab was selected so as the surface energy estimate would comply with known values. For a 15.3724 Å thick slab (12 atomic layers) the surface energy was 151.6 meV/Å^2, which agrees with the values calculated in [47,48]: 155.9 meV/Å^2 and 149.2 meV/Å^2, respectively. In order to ensure, that the slab of the chosen thickness reasonably represents the properties of macroscopic crystal surface, it was additionally tested for convergence of Li binding energies. The binding energy of a lithium atom in T3 position (see Fig. 1) was calculated with the slabs of 12 and 11 layers thickness. The values occurred to be 1.24 eV and 1.201 eV respectively, making difference of only 3.15%.

A plane-wave energy cut-off of 245.3 eV was used in the calculations. All structural optimizations were carried out until the forces, acting on atoms, fell below 0.01 eV/Å.

At first, the behavior of Li atoms on the surface was investigated. A set of structures with different lithium atom positions were calculated, and after that the most energetically favorable positions of lithium on Si (100) were determined (Fig. 1).

The lithium binding energies (Table 1) were calculated as:

$$E = (E_{\text{SiLi}} - E_{\text{Si(100)}} - nE_{\text{Li}})/n, \tag{1}$$

where E_{SiLi} is the full energy of Si (100) surface with lithium atoms adsorbed, $E_{\text{Si}}(100)$ – the full energy of a silicon supercell with two reconstructed (100) surfaces, E_{Li} – potential energy per atom in lithium crystal, n – the number of lithium atoms adsorbed.

As can be seen in Table 1, the most energetically favorable position is T3, with lithium atom placed in a valley between silicon dimers (Fig. 1), which is in agreement with other theoretical studies [49]. It is worth noting that lithium binding energy decreases
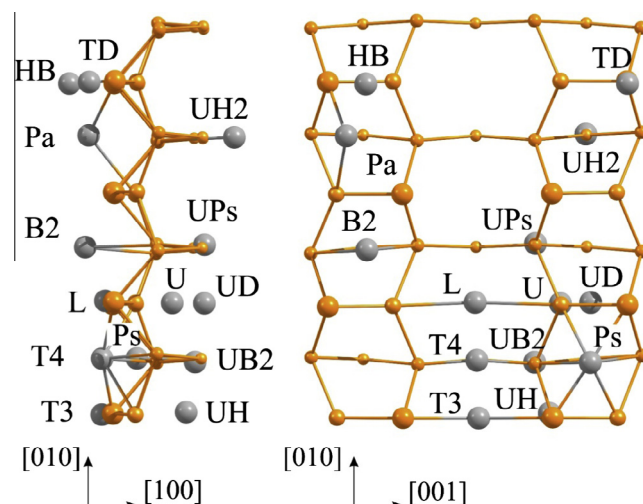
Fig. 1. Different positions of lithium atom on Si (100) surface and in subsurface layers. Silicon atoms are in orange color, lithium – light gray. Left panel - side view, right panel - top view.

Table 1
Binding energies of lithium atom adsorbed on Si (100) surface at different positions.

| Li position	Li atom on Si (100) surface binding energy, eV
Surface	
T3	−1.240
L	−1.177
T4	−1.160
Ps	−1.045
B2	−1.045
Pa	−1.040
HB	−0.518
TD	−0.517
Subsurface	
UPs	−1.037
UH	−0.810
UB2	−0.809
U	−0.793
UH2	−0.761
UD	−0.110

when lithium atom propagates into silicon (positions UD, UH, UH2, UB2, U) or goes out of the valley (positions HB, TD). Hence, the position between silicon dimers can be considered as the preferable initial lithium atom location. To support this thesis, transitions between surface and subsurface positions were simulated (Fig. 2).

The heights of the potential barriers shown in Fig. 2 argue that lithium can easily migrate on the surface at room temperature, but is unlikely to go below the surface. So lithium atoms are kept in the surface-adsorbed positions by the high potential barriers. It is worth noting that the barriers of migration under the surface are lower and are comparable with the migration barriers in bulk silicon, obtained from theoretical calculations (0.85 eV for a cubic silicon supercell containing 64 atoms) and experiment (0.8 eV [13]).

At small lithium concentrations, two different paths of migration from surface to subsurface layers can be figured out:

(1) T3 → UH → UB2, further referred as [T3 → UB2]
(2) L → U → UB2, further referred as [L → UB2]

The initial positions are considered to be T3 and L, with a possibility of hopping between them (the activation energies are 0.43 eV from T3 to L and 0.37 eV backwards). The energy of the system is 0.063 eV lower, when lithium is in T3, and the barriers for lithium going below the surface T3 → UH and L → U are much
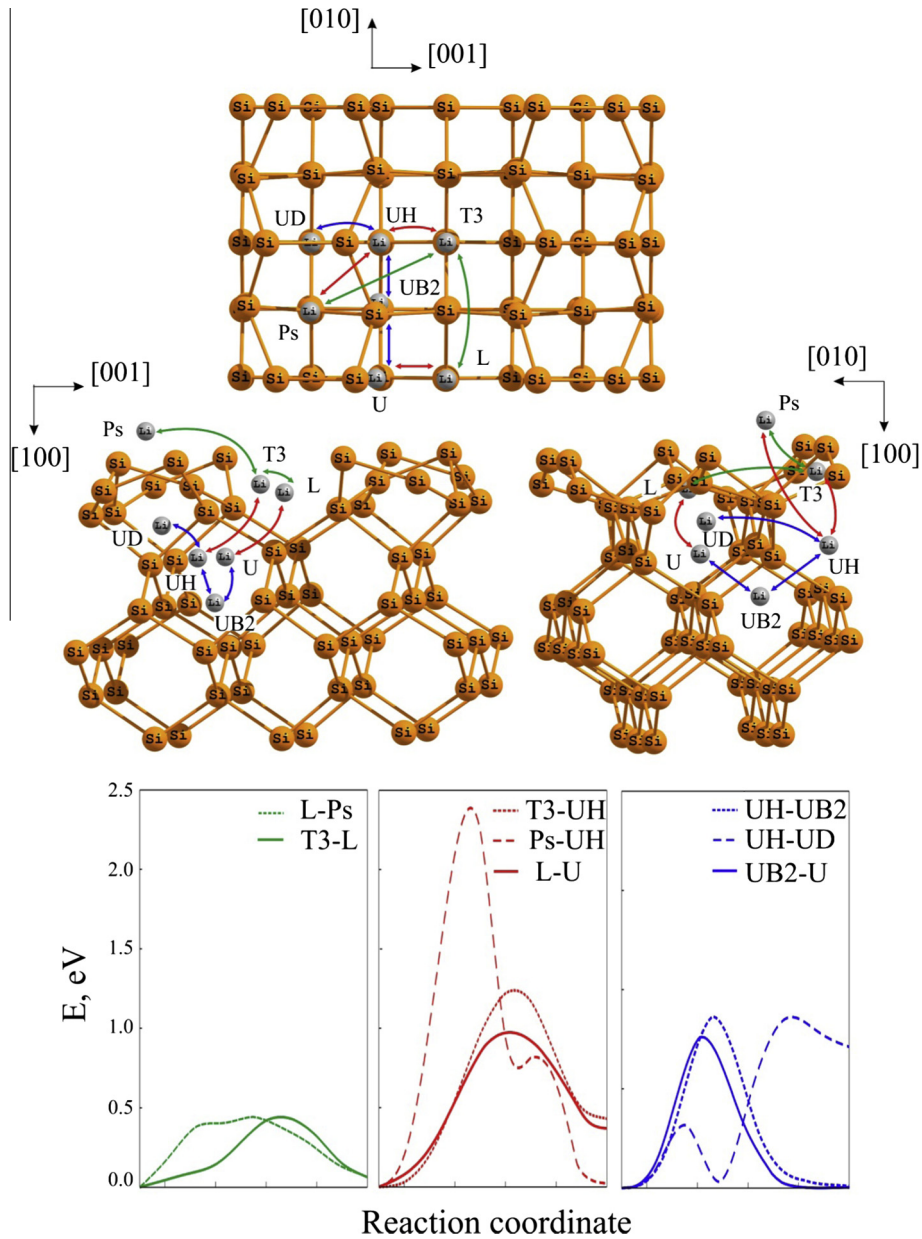
Fig. 2. Transition paths between surface and subsurface positions of lithium on Si (1 0 0) surface. Top and middle panels – top and side views. Bottom panel – potential energy along the transition paths.

greater than for migrating on the surface. The possible paths of a lithium atom are shown in Fig. 2.

In silicon crystal, lithium atoms are located in tetrahedral pores. Hence, a lithium atom that reaches position UB2, which is similar to a tetrahedral pore, can be considered to be in bulk.

The rate constants of lithium jumps between positions X1 and X2 were found as:

$$K(X1 \rightarrow X2) = \frac{k_b T}{h} \cdot exp\left(-\frac{E_b}{k_b \cdot T}\right)$$

where k_b is the Boltzmann constant, h is the Plank constant, E_b is the energy barrier between positions X1 and X2 and T is the temperature.

The probability of a jump in a forward direction is:

$$p(X1 \rightarrow X2) = \frac{K(X1 \rightarrow X2)}{K(X2 \rightarrow X1)}$$

Four paths of lithium atom transition into bulk silicon were compared:

$$[L \rightarrow UB2] = w(L)p(L \rightarrow U)p(U \rightarrow UB2)$$

$$[T3 \rightarrow UB2] = w(T3)p(T3 \rightarrow UH)p(UH \rightarrow UB2)$$

Here, w(L) and w(T3) are the occupancies of T3 and L estimated by the Gibbs distribution:

$$w(E_i) = \frac{e^{-\Delta E_i/k_b T}}{e^{-\Delta E(T3)/k_b T} + e^{-\Delta E(L)/k_b T}}$$

where i denotes T3 or L, ΔE_i is the surface binding energy of Li atom in T3 or L site. At room temperature, the occupancies are w(T3) = 0.5157 and w(L) = 0.4843.

The ratio between the numbers of lithium atoms penetrating below the surface along these paths can be found as:

$$P_1\{[L \to UB2]\} = \frac{[L \to UB2]}{\sum[X1 \to X2]}$$

$$P_2\{[T3 \to UB2]\} = \frac{[T3 \to UB2]}{\sum[X1 \to X2]}$$

where $\sum[X1 \to X2] = [L \to UB2] + [T3 \to UB2]$.

The relation between transitions along these two paths at different temperatures is shown in Fig. 3. When silicon is used as anode material in Li-ion batteries, the operating temperatures are always lower than 400 K. As can be seen from Fig. 3, in this case $L \to U \to UB2$ is the preferable path for the lithium migration into bulk silicon.

After that, we made a suggestion that the potential barriers of lithium atom transitions below the surface will decrease at greater concentrations of lithium on the surface. Structures with different degrees of Si (100) filling were calculated. Lithium atoms were initially placed into positions T3, L and Ps, as the most energetically favorable, and then the geometry was optimized.

As the concentration rises, lithium atoms gather into small clusters (with minimal Li–Li distance of 2.75 Å), which agrees with other experimental [50–52] and theoretical investigations [53,54]. However, it appears that the lithium binding energies fall with the concentration level increasing, see Table 2. This trend can be explained by the Coulomb interactions between positively charged lithium ions, which are increasing with the surface filling. It also should be noted, that surface reconstruction changes from the antisymmetric silicon dimer arrangement to a symmetric one; this was previously observed in [53,54].

In order to find out, how the diffusion through the surface is affected by the degree of surface filling, the heights of T3–UH and L_U/U_UB2 transition barriers were calculated (Table 3). For the symmetric silicon dimer arrangement these two paths are equivalent.

As seen from the table, with the rise of lithium concentration on Si (100) surface, the potential barrier for $T3 \to UH$ transition has a trend to fall, although the situation does not change significantly. However, when the filling reaches 2 ML, lithium atoms go into the bulk easier than in the backward direction. That indicates the beginning of effective diffusion.
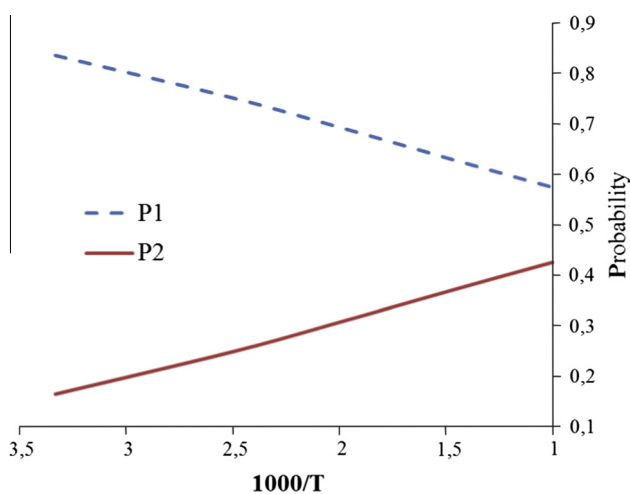
Table 2
Lithium binding energies on Si (100) surface in different atom positions and at different degrees of surface filling.

Li atoms positions	Degree of surface filling, monolayers (ML)	Binding energy per lithium atom (eV)
L[a]	0.25	−0.989
T3[a]	0.25	−0.996
Ps[a]	0.50	−0.778
T3, L[a]	0.50	−0.936
T3, Ps[a]	0.75	−0.990
L, Ps[a]	0.75	−0.990
T3, L, Ps[b]	1.00	−1.084
T3, L, Ps, HB[b]	1.50	−0.564
T3, L, Ps, 0.5TD[b]	1.50	−0.518
T3, L, Ps, TD[b]	2.00	−0.454

[a] Antisymmetric silicon dimer arrangement.
[b] Symmetric silicon dimer arrangement.

Table 3
Potential barrier heights for lithium transition along T3-UH and L_U paths with respect to the degree of Si (100) surface filling.

Li atoms positions	Degree of surface filling, monolayers (ML)	Transition potential barrier (eV)	
		Forward	Backward
T3 (single atom, T3-UH)	0.03	1.22	0.79
L (single atom, L_U)	0.03	0.89	0.52
T3, L (T3-UH)	0.50	1.39	0.61
T3, L (L_U)	0.50	0.88	0.71
T3, Ps(T3-UH)	0.75	1.07	0.84
L, Ps(T3-UH)	0.75	1.09	0.85
T3, L, Ps(T3-UH)	1.00	1.02	0.68
T3, L, Ps, HB(T3-UH)	1.50	0.98	0.72
T3, L, Ps, TD(T3-UH)	2.00	0.99	1.10

3. Dynamics of lithium diffusion into bulk silicon

3.1. Development of empirical potential

Since DFT calculations are very computationally expensive, direct molecular dynamical modeling of diffusion even in small lithium–silicon systems is impossible. Empirical interatomic potentials can considerably extend capabilities of computer modeling. For this purpose the interactions between atoms are found not out of the principles of quantum chemistry, but with an over-simplified scheme of a classical form.

Only one empirical potential has been developed for silicon–lithium systems by now [55]. However, this potential, like the others developed with only macroscopic silicon crystal properties as a reference [56], is unable to reproduce forces acting on atoms with local environment distorted away from the equilibrium (see Table 4). In this work, a new empirical potential was developed so as to correctly describe the atomic forces in systems with a surface, with a large number of vacancies and with different concentrations of lithium atoms in silicon. This potential was used to describe the diffusion process at the level of individual atoms. Adjustable parameters of the proposed potential were found using the force-matching method [57]. The potential is based on angular dependent potential (ADP) proposed by Mishin [58], an extended version of embedded atom model (EAM [59,60]). In this approach, the potential energy of the system is a sum of individual contributions from each atom, calculated by the formula:

$$E_i = F_\alpha \left(\sum_{j \neq i} \rho_\beta(r_{ij}) \right) + \frac{1}{2} \sum_{j \neq i} \varphi_{\alpha\beta}(r_{ij}) + \frac{1}{2} \sum_s (\mu_i^s)^2 + \left(\frac{1}{2} \sum_{s,t} (\lambda_i^{st})^2 - \frac{1}{6} \nu_i^2 \right)$$

Fig. 3. Probabilities of lithium atom transitions along P1 or P2 path.

$$\mu_i^s = \sum_{j \neq i} u_{\alpha\beta}(r_{ij})r_{ij}^s$$

$$\lambda_i^{st} = \sum_{j \neq i} w_{\alpha\beta}(r_{ij})r_{ij}^s r_{ij}^t$$

$$\nu_i = \sum_s \lambda_i^{ss}$$

where E_i is ith atom contribution to the total potential energy of the system, r_{ij} – vector pointing from ith atom to jth or its length, α and β – the species of ith and jth atoms correspondingly, s and t run over x, y, z components of vectors or tensors. F_α, ρ_β, $\varphi_{\alpha\beta}$, $u_{\alpha\beta}$ and $w_{\alpha\beta}$ are some functions subject to the potential fitting procedure. Details about the ADP potential may be found in [58].

Table 4
Root mean squared (RMS) errors in calculating forces and energies for structures from the DFT-calculated reference database with different potentials: Stillinger–Weber (SW, [63]), Tersoff [64], EDIP [65], 2NNMEAM [55], ADP (this work). The values in percentages are the ratios of the RMS error to RMS absolute values of force or energy in the database. The potentials were compared separately for the parts of the reference database containing only silicon structures, only lithium structures and only structures of silicon and lithium compounds.

	RMS errors in forces (eV/Å)		RMS errors in energies (eV)	
SW(Si only)	2.236	165%	130.3	25.4%
Tersoff(Si only)	2.357	174%	105.7	20.7%
EDIP(Si only)	1.856	137%	80.6	15.7%
2NNMEAM(Si only)	2.015	150%	105.6	21%
ADP(Si only)	0.477	33.9%	6.8	1.3%
ADP(Li only)	0.283	15.7%	3.5	1.1%
ADP(Si–Li)	0.377	26.5%	5.2	1.4%

To use the ADP potential for monoatomic systems (e.g. only silicon atoms), one has to define 5 functions: 3 from the EAM model – $\rho_{Si}(r_{ij})$, $F_{Si}(\rho_i)$, $\varphi_{Si-Si}(r_{ij})$; and 2 functions added in the ADP model - $u_{Si-Si}(r_{ij})$ and $w_{Si-Si}(r_{ij})$. For binary systems (Si and Li), 13 functions are needed: 5 functions to describe interactions between Si atoms, 5 – between Li atoms, and 3 – between Si–Li pairs: $\varphi_{Si-Li}(r_{ij})$, $u_{Si-Li}(r_{ij})$ and $w_{Si-Li}(r_{ij})$. In this work, only minimal assumptions were made about the form of these functions, because the more generic form functions have, the more freedom force-matching algorithm has. For this purpose the functions were represented as polynomials subject only to boundary conditions (e.g. functions and first derivatives zeroing out at $r_{ij} \geqslant R_{cut}$, where $R_{cut} = 4.9$ Å is a force cut-off radius). Thus these 13 functions were represented by 67 adjustable parameters. However, this particular parameterization form was actually never used in MD calculations: once the potential functions were fitted, they were turned into the tabulated LAMMPS potential file format.

For determining the optimal parameters of the potential, which will give the most accurate description of interatomic forces, the parameters were fitted against a reference database of structures with DFT calculated forces and energies. The database included periodic structures of $Si_{62}Li_2$, $Si_{16}Li_{30}$, $Si_{16}Li_{59}$, Si_{189} (pseudo-amorphous silicon) previously obtained in studies of lithium diffusion in bulk and amorphous silicon [61]; spherical nanoparticles Si_{75}, Si_{160}, Li_{77} and Li_{168} with large fraction of surface atoms; supercells of silicon ($2 * 2 * 2$ cubic unit cells) and lithium ($3 * 3 * 3$ cubic unit cells) with 1 vacancy per each (Si_{63} and Li_{53}). While modeling nanoparticles, a 13 Å vacuum spacing was used to prevent them from interacting with their periodical images. In other cases, the volume corresponded to the one of the ground state.

Aiming at the reference structures containing as many different variants of atomic coordination as possible, the structures were calculated by MD modeling of high temperature (1000–1800 K)

atomic motion. Not all the time iterations of the MD were used to build up the reference database: geometrical configurations at only each tenth time iterations were picked, so that the atomic positions had changed significantly from the previously selected configuration. The database of reference structures also contained some iterations of geometrical relaxation in pure silicon or lithium crystal under uniaxial or shear strain (up to 12%).

In total, 141 geometrical structures were calculated: 59 structures for fitting silicon potential functions ($\rho_{Si}(r_{ij})$, $F_{Si}(\rho_i)$, $\varphi_{Si-Si}(r_{ij})$, $u_{Si-Si}(r_{ij})$ and $w_{Si-Si}(r_{ij})$), 34 – for lithium potential functions and 48 – for silicon–lithium cross potential functions. The calculated forces and energies of these structures were taken to be a reference during potential parameters fitting.

For any trial set of parameters a residual function Z was calculated:

$$Z = \sum (F_{EMP} - F_{VASP})^2 + k_{F-E} \sum (E_{EMP} - E_{VASP})^2$$

$$Z \rightarrow \min$$

where F_{emp} and E_{emp} are forces and energies calculated with the trial ADP potential, F_{VASP} and E_{VASP} – corresponding DFT values, k_{E-F} – coefficient, which equalizes the contributions to Z from discrepancies in the forces and the energies. The global minimum of Z corresponds to the optimal set of parameters. The minimization of Z was conducted in 2 steps: first, the areas, where the global minimum is likely to be situated, were found using a genetic algorithm, starting from a random initial population; second, the local minima in those areas were located by Levenberg–Marquardt algorithm [62]. The lowest of the resulting minima was assumed to be the global minimum. The fitted functions of the resulting potential can be found in Appendix A.

The developed potential adequately reproduces interactions between atoms in pure silicon, lithium and their compounds. Root mean squared (RMS) errors in calculating forces and energies for structures from the reference database are listed in Table 4. The potential is compared against other popular potentials for silicon and the potential from [55]. The values of the RMS error were compared to RMS magnitude of forces and RMS energy of the database.

The comparison between DFT and ADP calculated Li binding energies in T3 and L sites and transition barriers is summarized in Table 5. The overall agreement in the values allows us to rely on the qualitative results obtained by MD calculations with the proposed potential in this particular case (simulation of Li penetration through Si (100) surface) and even to make rough estimates of such values as diffusion coefficient.

3.2. Simulations of lithium diffusion into bulk silicon

The ADP potential developed in this work was used for modeling lithium diffusion from liquid into silicon through (100) surface with LAMMPS MD software package [66,67]. The simulation cell had size of $27 * 27 * 80$ Å and was subject to periodical boundary conditions in x and y directions. The simulation cell walls

Table 5
Comparison of Li atom binding energies and transition barriers calculated by DFT and by the proposed ADP potential.

	DFT calculated, eV	ADP calculated, eV
Li atom binding energy at positions		
T3	−1.24	−1.38
L	−1.177	−1.341
Li atom transition barrier energy		
T3-UH	1.222	1.023
UH-UB2	0.847	0.826
T3-UH (2 ML coating)	0.989	1.185

perpendicular to the non-periodic z direction were set to be reflective in order to prevent atoms from flying away out of the cell. It contained 1000 silicon atoms forming a slab ($5*5*5$ unit cells) and 1200 lithium atoms placed right above silicon (1 0 0) surface (see Fig. 4). The lower part of the silicon slab, 4 bottom layers or 4.9 Å (which is a cut-off distance for the potential), was frozen. MD was run under Nose–Hoover thermostat [68] at different temperatures from 500 to 800 K with a timestep of 0.5 fs for a period of 10 ns.

During the simulations, lithium atoms migrated down along z direction, occupying tetrahedral pores in silicon. It was observed throughout the process, that lithium penetrated silicon in a layer-by-layer way, filling horizontal planes containing tetrahedral pores one by one: Li atoms were unlikely to go deeper into silicon crystal until the whole plane was filled. Thus a sharp flat boundary between undoped silicon and SiLi phase persisted.

Basing on the first Fick's law $J = -D\frac{\partial C}{\partial z}(x)$ the diffusion coefficient D was found. The diffusion flux J was calculated as the number of Li atoms going through a horizontal plane in a certain period of time (0.5 ns). This value occurred to be nearly constant for different planes and different moments of time. The concentration gradient $\frac{\partial C}{\partial z}$ was calculated with the assumption that concentration rises sharply from 0 in undoped silicon to the value, corresponding to SiLi phase, at a distance of only one atomic layer (distance between planes containing tetrahedral pores – 1.35 Å). The temperature dependence of the diffusion coefficient is shown in Fig. 5. The results were interpolated by the formula:

$$D = 5 \times 10^{-04} \times \exp(-0.375/k_b T),$$

which shows that the effective migration barrier is 0.375 eV.

The mechanism of the layer-by-layer penetration into the crystal with a sharp phase boundary was the following. At first, one Li atom entered a pore below the phase boundary, thereby deforming the neighboring lattice and causing silicon–silicon bonds extension in the direction, perpendicular to the crystal surface. The average Si–Si distance rose from 2.35 Å to 2.55 Å, apparently causing a decrease in the barriers for Li migration into the adjacent pores. The effect of neighboring pores occupation on Li migration was previously investigated by the DFT calculations in [70]: when the pore with a Li atom inside is surrounded by 0, 1, 2 or 3 occupied pores, the barriers for this Li atom migration into a neighboring (unoccupied) pore are 0.903, 0.735, 0.477 and 0.362 eV, correspondingly. After the adjacent pores were deformed, they were soon occupied too and the lattice deformation spread further across the horizontal plane, leading to a full plane filling and Si–SiLi phase boundary propagation. Among other things, it is worth noting that the elongation of Si–Si bonds and changing of the angles between them caused swelling of the slab by 35%, which can be considered as a possible origin of mechanical stress.
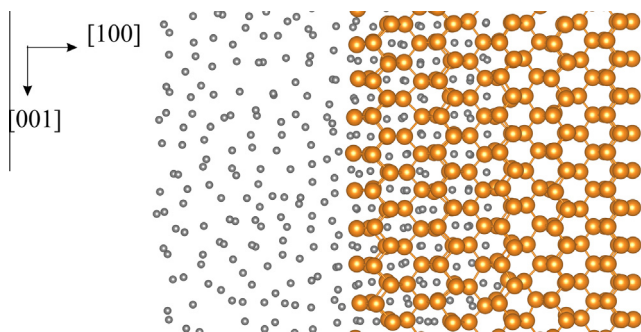

Fig. 4. Lithium diffusion into silicon through (1 0 0) surface after 2 ns of MD at 600 K. Lithium atoms are in light gray, silicon atoms are in orange. View along [0 1 1].
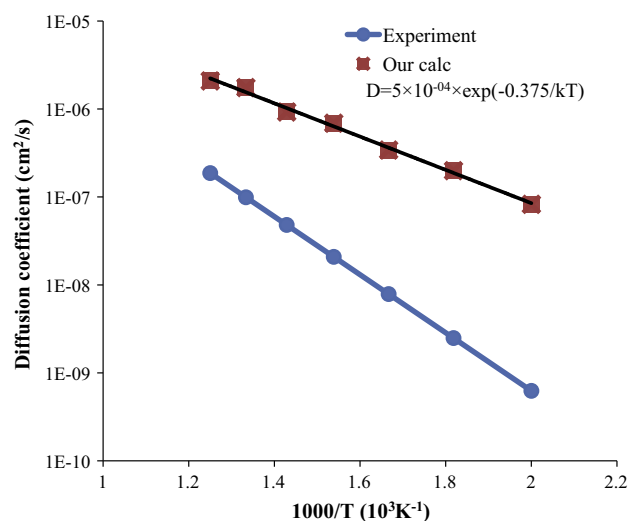

Fig. 5. Coefficient of Li diffusion into silicon with respect to temperature T, calculated by MD with the ADP potential, and obtained from the experiment [69].

Overall, it can be concluded, that the rate of diffusion in SiLi is higher than in undoped silicon, and the rate of Li penetrating into pure silicon is the limiting factor of the diffusion.
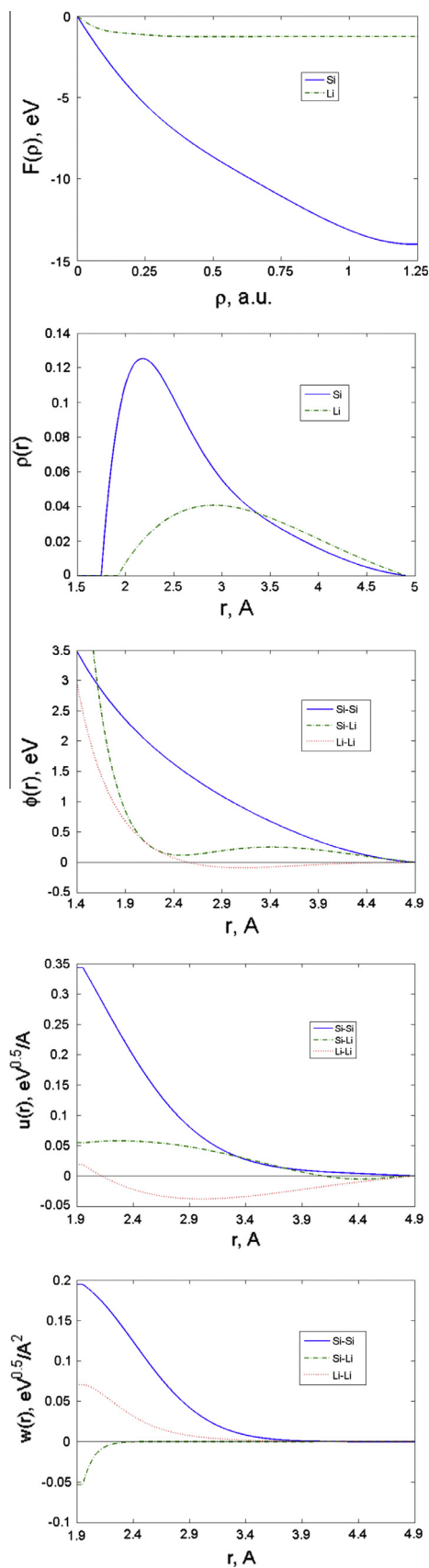
4. Conclusion

The results of the investigations show that, when lithium concentration on silicon (1 0 0) surface is low, single lithium atoms are unlikely to migrate into the crystal, as the binding energies of Li atoms in surface positions are higher than in subsurface layers. At Li-ion battery operating temperatures, the potential barrier for Li transition from surface to subsurface layer is equal to the barrier of the limiting stage, i.e. migration along the L → UB2 path. Its height is slightly larger than the height of the barrier for a single Li atom migration in bulk silicon (0.89 eV and 0.85 eV correspondingly). When the silicon surface is covered by 2 monolayers of lithium, the conditions for Li atoms migrating below the surface are more favorable, because the subsurface states are more stable than the positions on the surface. Besides this, with the rise of Li concentration, the form of the surface reconstruction changes from the antisymmetric silicon dimer arrangement to the symmetric one. As a result, the possible migration paths, T3 → UH and L → U, become equivalent and the number of possible transitions increases. Thus quantum-chemical modeling explains the experimental observations of small diffusion rates at the first stage of the process, which is related to overcoming the surface.

By the means of empirical MD simulations, it was found out that, after lithium overcomes the surface, its propagation into the bulk proceeds in a layer-by-layer way and is accompanied by volume expansion. In this process, the widening of the pores, through which Li atoms migrate, and appearance of other Li atoms in the adjacent pores causes decrease in the migration barriers (0.362–0.375 eV) and consequently increase in the diffusion rate.

Acknowledgments

Appendix A.

See Fig. A.1.

Appendix B. Supplementary material

Supplementary data associated with this article can be found, in the online version, at http://dx.doi.org/10.1016/j.commatsci.2015.06.024.

References

[1] V.P. Nikolaev, A.G. Morachevskii, A.I. Demidov, E.V. Bairachnyi, J. Appl. Chem. USSR 53 (9) (1980) 1549–1551.
[2] B.A. Boukamp, G.C. Lesh, R.A. Huggins, J. Electrochem. Soc. 128 (4) (1981) 725–729, http://dx.doi.org/10.1149/1.2127495.
[3] H. Okamoto, J. Phase Equilib. 11 (3) (1990) 306–312, http://dx.doi.org/10.1007/BF03029305.
[4] M.N. Obrovac, L. Christensen, Electrochem. Solid-State Lett. 7 (5) (2004) A93–A96, http://dx.doi.org/10.1149/1.1652421.
[5] U. Kasavajjula, C. Wang, A.J. Appleby, J. Power Sources 163 (2) (2007) 1003–1039, http://dx.doi.org/10.1016/j.jpowsour.2006.09.084.
[6] R.A. Huggins, J. Power Sources 81 (1999) 13–19, http://dx.doi.org/10.1016/S0378-7753(99)00124-X.
[7] L.Y. Beaulieu, K.W. Eberman, R.L. Turner, L.J. Krause, J.R. Dahn, Electrochem. Solid-State Lett. 4 (9) (2001) A137–A140, http://dx.doi.org/10.1149/1.1388178.
[8] A. Anani, S. Crouch-Baker, R.A. Huggins, J. Electrochem. Soc. 134 (12) (1987) 3098–3102, http://dx.doi.org/10.1149/1.2100347.
[9] C.J. Wen, R.A. Huggins, J. Solid State Chem. 37 (3) (1981) 271–278, http://dx.doi.org/10.1016/0022-4596(81)90487-4.
[10] H. Li, X. Huang, L. Chen, G. Zhou, Z. Zhang, D. Yu, N. Pei, Solid State Ionics 135 (1) (2000) 181–191, http://dx.doi.org/10.1016/S0167-2738(00)00362-3.
[11] J.O. Besenhard, J. Yang, M. Winter, J. Power Sources 68 (1) (1997) 87–90, http://dx.doi.org/10.1016/S0378-7753(96)02547-5.
[12] A.S. Fedorov, Z.I. Popov, A.A. Kuzubov, S.G.E. Ovchinnikov, JETP Lett. 95 (3) (2012) 143–147, http://dx.doi.org/10.1134/S0021364012030058.
[13] H. Bracht, N.A Stolwijk, 2 Diffusion in Si, in: Diffusion in Semiconductors, Springer, Berlin Heidelberg, 1998, pp. 12–134, http://dx.doi.org/10.1007/10426818_4.
[14] T. Takamura, S. Ohara, M. Uehara, J. Suzuki, K. Sekine, J. Power Sources 129 (1) (2004) 96–100, http://dx.doi.org/10.1016/j.jpowsour.2003.11.014.
[15] J. Yin, M. Wada, K. Yamamoto, Y. Kitano, S. Tanase, T. Sakai, J. Electrochem. Soc. 153 (3) (2006) A472–A477, http://dx.doi.org/10.1149/1.2160429.
[16] Q. Zhang, W. Zhang, W. Wan, Y. Cui, E. Wang, Nano Lett. 10 (9) (2010) 3243–3249, http://dx.doi.org/10.1021/nl904132v.
[17] C.K. Chan, H. Peng, G. Liu, K. McIlwrath, X.F. Zhang, R.A. Huggins, Y. Cui, Nat. Nanotechnol. 3 (1) (2007) 31–35, http://dx.doi.org/10.1038/nnano.2007.411.
[18] K. Peng, J. Jie, W. Zhang, S.T. Lee, Appl. Phys. Lett. 93 (3) (2008) 033105, http://dx.doi.org/10.1063/1.2929373.
[19] X.H. Liu, L.Q. Zhang, L. Zhong, Y. Liu, H. Zheng, J.W. Wang, J.Y. Huang, Nano Lett. 11 (6) (2011) 2251–2258, http://dx.doi.org/10.1021/nl200412p.
[20] N. Dimov, S. Kugino, M. Yoshio, Electrochim. Acta 48 (11) (2003) 1579–1587, http://dx.doi.org/10.1016/S0013-4686(03)00030-6.
[21] H. Kim, M. Seo, M.H. Park, J. Cho, Angew. Chem. Int. Ed. 49 (12) (2010) 2146–2149, http://dx.doi.org/10.1002/anie.200906287.
[22] C.K. Chan, R.N. Patel, M.J. O'Connell, B.A. Korgel, Y. Cui, ACS Nano 4 (3) (2010) 1443–1450, http://dx.doi.org/10.1021/nn901409q.
[23] M.H. Park, M.G. Kim, J. Joo, K. Kim, J. Kim, S. Ahn, J. Cho, Nano Lett. 9 (11) (2009) 3844–3847, http://dx.doi.org/10.1021/nl902058c.
[24] T. Song, J. Xia, J.H. Lee, D.H. Lee, M.S. Kwon, J.M. Choi, U. Paik, Nano Lett. 10 (5) (2010) 1710–1716, http://dx.doi.org/10.1021/nl100086e.
[25] S. Zhou, D. Wang, ACS Nano 4 (11) (2010) 7014–7020, http://dx.doi.org/10.1021/nn102194w.
[26] S.H. Ng, J. Wang, D. Wexler, K. Konstantinov, Z.P. Guo, H.K. Liu, Angew. Chem. Int. Ed. 45 (41) (2006) 6896–6899, http://dx.doi.org/10.1002/anie.200601676.
[27] H. Kim, B. Han, J. Choo, J. Cho, Angew. Chem. 120 (52) (2008) 10305–10308, http://dx.doi.org/10.1002/ange.200804355.
[28] Y. Yao, M.T. McDowell, I. Ryu, H. Wu, N. Liu, L. Hu, Y. Cui, Nano Lett. 11 (7) (2011) 2949–2954, http://dx.doi.org/10.1021/nl201470j.
[29] X.L. Wang, W.Q. Han, ACS Appl. Mater. Interfaces 2 (12) (2010) 3709–3713, http://dx.doi.org/10.1021/am100857h.

Fig. A.1. The functions of the proposed potential. From top to bottom: F_α, ρ_β, $\varphi_{\alpha\beta}$, $u_{\alpha\beta}$, $w_{\alpha\beta}$.

[30] C.Y. Sun, C. Qin, C.G. Wang, Z.M. Su, S. Wang, X.L. Wang, E.B. Wang, Adv. Mater. 23 (47) (2011) 5629–5632, http://dx.doi.org/10.1002/adma.201102538.

[31] Y. Qu, L. Liao, Y. Li, H. Zhang, Y. Huang, X. Duan, Nano Lett. 9 (12) (2009) 4539–4543, http://dx.doi.org/10.1021/nl903030h.

[32] A. Magasinski, P. Dixon, B. Hertzberg, A. Kvit, J. Ayala, G. Yushin, Nat. Mater. 9 (4) (2010) 353–358, http://dx.doi.org/10.1038/nmat2725.

[33] M. Ge, J. Rong, X. Fang, C. Zhou, Nano Lett. 12 (5) (2012) 2318–2323, http://dx.doi.org/10.1021/nl300206e.

[34] H. Kleine, M. Eckhardt, D. Fick, Surf. Sci. 329 (1) (1995) 71–76, http://dx.doi.org/10.1016/0039-6028(95)00120-4.

[35] B. Peng, F. Cheng, Z. Tao, J. Chen, J. Chem. Phys. 133 (3) (2010) 034701, http://dx.doi.org/10.1063/1.3462998.

[36] G. Kresse, J. Hafner, Phys. Rev. B 47 (1) (1993) 558, http://dx.doi.org/10.1103/PhysRevB.47.558.

[37] G. Kresse, J. Hafner, Phys. Rev. B 49 (20) (1994) 14251, http://dx.doi.org/10.1103/PhysRevB.49.14251.

[38] G. Kresse, J. Furthmüller, Phys. Rev. B 54 (16) (1996) 11169, http://dx.doi.org/10.1103/PhysRevB.54.11169.

[39] P. Hohenberg, W. Kohn, Phys. Rev. 136 (3B) (1964) B864, http://dx.doi.org/10.1103/PhysRev.136.B864.

[40] W. Kohn, L.J. Sham, Phys. Rev. 140 (4A) (1965) A1133, http://dx.doi.org/10.1103/PhysRev.140.A1133.

[41] P.E. Blöchl, Phys. Rev. B 50 (24) (1994) 17953, http://dx.doi.org/10.1103/PhysRevB.50.17953.

[42] G. Kresse, D. Joubert, Phys. Rev. B 59 (3) (1999) 1758, http://dx.doi.org/10.1103/PhysRevB.59.1758.

[43] J.P. Perdew, K. Burke, M. Ernzerhof, Phys. Rev. Lett. 77 (18) (1996) 3865, http://dx.doi.org/10.1103/PhysRevLett.77.3865.

[44] S. Grimme, J. Comput. Chem. 27 (15) (2006) 1787–1799, http://dx.doi.org/10.1002/jcc.20495.

[45] G. Henkelman, B.P. Uberuaga, H. Jónsson, J. Chem. Phys. 113 (22) (2000) 9901–9904, http://dx.doi.org/10.1063/1.1329672.

[46] H.J. Monkhorst, J.D. Pack, Phys. Rev. B 13 (12) (1976) 5188, http://dx.doi.org/10.1103/PhysRevB.13.5188.

[47] Y. Enta, S. Suzuki, S. Kono, Surf. Sci. 242 (1) (1991) 277–283, http://dx.doi.org/10.1016/0039-6028(91)90279-2.

[48] T. Tabata, T. Aruga, Y. Murata, Surf. Sci. 179 (1) (1987) L63–L70, http://dx.doi.org/10.1016/0039-6028(87)90114-2.

[49] S.C. Jung, Y.K. Han, Phys. Chem. Chem. Phys. 13 (48) (2011) 21282–21287, http://dx.doi.org/10.1039/C1CP22026H.

[50] M.J. Johansson, S.M. Gray, L.S.O. Johansson, Phys. Rev. B 53 (3) (1996) 1362, http://dx.doi.org/10.1103/PhysRevB.53.1362.

[51] L.S.O. Johansson, T.M. Grehk, S.M. Gray, M. Johansson, A.S. Flodström, Nucl. Instrum. Methods Phys. Res. Sect. B 97 (1) (1995) 364–367, http://dx.doi.org/10.1016/0168-583X(94)00364-5.

[52] T.M. Grehk, L.S.O. Johansson, S.M. Gray, M. Johansson, A.S. Flodström, Phys. Rev. B 52 (23) (1995) 16593, http://dx.doi.org/10.1103/PhysRevB.52.16593.

[53] H.Q. Shi, M.W. Radny, P.V. Smith, Surf. Sci. 574 (2) (2005) 233–243, http://dx.doi.org/10.1016/j.susc.2004.10.046.

[54] Y.J. Ko, K.J. Chang, J.Y. Yi, Phys. Rev. B 56 (15) (1997) 9575, http://dx.doi.org/10.1103/PhysRevB.56.9575.

[55] Z. Cui, F. Gao, Z. Cui, J. Qu, J. Power Sources 207 (2012) 150–159, http://dx.doi.org/10.1016/j.jpowsour.2012.01.145.

[56] H. Balamane, T. Halicioglu, W.A. Tiller, Phys. Rev. B 46 (4) (1992) 2250, http://dx.doi.org/10.1103/PhysRevB.46.2250.

[57] F. Ercolessi, J.B. Adams, EPL (Europhys. Lett.) 26 (8) (1994) 583, http://dx.doi.org/10.1209/0295-5075/26/8/005.

[58] Y. Mishin, M.J. Mehl, D.A. Papaconstantopoulos, Acta Mater. 53 (15) (2005) 4029–4041, http://dx.doi.org/10.1016/j.actamat.2005.05.001.

[59] M.S. Daw, M.I. Baskes, Phys. Rev. Lett. 50 (17) (1983) 1285, http://dx.doi.org/10.1103/PhysRevLett.50.1285.

[60] M.S. Daw, M.I. Baskes, Phys. Rev. B 29 (12) (1984) 6443, http://dx.doi.org/10.1103/PhysRevB.29.6443.

[61] Z.I. Popov, A.S. Fedorov, A.A. Kuzubov, T.A. Kozhevnikova, J. Struct. Chem. 52 (5) (2011) 861–869, http://dx.doi.org/10.1134/S0022476611050039.

[62] D.W. Marquardt, J. Soc. Ind. Appl. Math. 11 (2) (1963) 431–441, http://dx.doi.org/10.1137/0111030.

[63] F.H. Stillinger, T.A. Weber, Phys. Rev. B 31 (8) (1985) 5262, http://dx.doi.org/10.1103/PhysRevB.31.5262.

[64] J. Tersoff, Phys. Rev. B 37 (12) (1988) 6991, http://dx.doi.org/10.1103/PhysRevB.37.6991.

[65] J.F. Justo, M.Z. Bazant, E. Kaxiras, V.V. Bulatov, S. Yip, Phys. Rev. B 58 (5) (1998) 2539, http://dx.doi.org/10.1103/PhysRevB.58.2539.

[66] S. Plimpton, J. Comput. Phys. 117 (1) (1995) 1–19, http://dx.doi.org/10.1006/jcph.1995.1039.

[67] http://lammps.sandia.gov.

[68] W.G. Hoover, Phys. Rev. A 31 (3) (1985) 1695, http://dx.doi.org/10.1103/PhysRevA.31.1695.

[69] E.M. Pell, Phys. Rev. 119 (4) (1960) 1222, http://dx.doi.org/10.1103/PhysRev.119.1222.

[70] A.A. Kuzubov, N.S. Eliseeva, Z.I. Popov, A.S. Fedorov, M.V. Serzhantova, V.M. Denisov, F.N. Tomilin, JETP Lett. 97 (11) (2013) 634–638, http://dx.doi.org/10.1134/S0021364013110088.